Short Cavity Erbium/Ytterbium Fiber Lasers Mode-Locked with a Saturable Bragg Reflector

Brandon C. Collings, Keren Bergman, *Member, IEEE,* S. T. Cundiff, Sergio Tsuda, J. Nathan Kutz, *Member, IEEE,* J. E. Cunningham, W. Y. Jan, M. Koch, and W. H. Knox

***Abstract*— We present short cavity erbium/ytterbium fiber lasers that are passively mode-locked with a saturable Bragg reflector. The lasers produce sub-500-fs pulses at fundamental cavity repetition rates as high as 300 MHz. Stable passive harmonic operation increases the repetition rate to 2.0 GHz. The mode-locking mechanism in both the normal and anomalous group velocity dispersion regimes is investigated using complete analytical and numerical models and direct comparison with the experimental results. A simple technique for accurately measuring the total cavity dispersion is presented.**

***Index Terms*— Mode-locked lasers, optical fiber communication, optical fiber lasers, optical pulse generation, optical solitons, quantum-well devices, rare-earth materials/devices, ultrafast optics.**

I. Introduction

HIGH-SPEED optical networks require sources producing ultrashort pulses at ever increasing repetition rates and average output powers. The 1550-nm wavelength region in silica fiber represents the lowest attenuation window where efficient, nearly quantum limited amplification is provided by Er-doped fiber amplifiers and soliton pulse propagation is supported. To be practical, these sources must be compact, reliable and require minimal power consumption. Mode-locked Er-doped fiber lasers, currently the subject of much research, provide potentially attractive short pulse sources possessing some key advantages over modulated continuous-wave (CW) sources including large optical bandwidths, high intensities and powers, short coherence lengths and high timing stability. The spectral bandwidth generated from a single mode-locked source can be partitioned to form a large number of wavelength-division multiplexed (WDM) channels, which may be economically advantageous over employment of multiple, individually selected distributed-feedback (DFB) lasers [1]. For applications in practical communication systems, mode-locked fiber lasers must demonstrate reliability and preferably be composed entirely of standard telecommunications certified components.

The mode-locking mechanism is central to the development of a competitive source. Several groups have successfully demonstrated passively mode-locked fiber lasers employing additive-pulse mode-locking (APM) which converts nonlinear self-phase modulation (SPM) into ultrafast amplitude modulation via an interferometer, as in the figure eight laser [2]–[8]. Another technique employs nonlinear polarization evolution in conjunction with a polarizer which also provides ultrafast amplitude modulation [9]. These mode-locking mechanisms are analogous to a fast saturable absorber and have typically been demonstrated in long length cavities (4–100 m), which can suffer from amplitude and timing jitter induced by environmental instabilities [10]. Fiber lasers have also been passively mode-locked in linear cavity configurations employing a semiconductor structure as the fast saturable absorber [11], [12]. The recently demonstrated saturable Bragg reflector (SBR) provides a self-starting mode-locking mechanism with minimal loss enabling efficient femtosecond mode-locking of low-gain lasers [13]–[16]. Because of this efficient mode-locking mechanism, a minimal amount of gain fiber and intracavity power is required. This allows the construction of shorter fiber laser cavities with higher fundamental repetition rates capable of generating subpicosecond pulses. This is the motivation behind the short (30–200 cm) fiber lasers discussed in this paper, which produce stable, self-starting high repetition rate pulse trains with wide optical bandwidths providing promising sources for high-speed TDM/WDM networks.

In this paper, we present several fiber lasers of various lengths mode-locked with SBR's with cavity dispersions in both the normal and anomalous (soliton) regimes. We also demonstrate passive harmonic mode-locking which produces stable, multigigabit femtosecond pulse trains. We study the dynamics of the SBR and mode-locking mechanism both experimentally and theoretically for several cavity configurations. Our model accounts for the formation dynamics of the pulse and its interaction with the SBR. Three separate time constants are used to model the SBR: an instantaneous response, a slow saturated response and a relaxation time. The overall temporal response of the SBR model closely matches experimental measurements obtained with pump-probe experiments. Our general mode-locking model predicts both the temporal and spectral pulse profiles with remarkable accuracy. We also present a simple method for accurately measuring the total group velocity dispersion of a complete

Manuscript received April 15, 1997. This work was supported by the National Science Foundation under Grant DMS-9508634 and Grant ECS-9502491, and by the Brazilian Conselho Nacional de Desenvolvimento Científico e Tecnológico.

B. C. Collings and K. Bergman are with Electrical Engineering, Princeton University, Princeton, NJ 08544 USA.

S. T. Cundiff, S. Tsuda, J. E. Cunningham, W. Y. Jan, and W. H. Knox are with Bell Laboratories, Lucent Technologies, Holmdel, NJ 07733 USA.

J. N. Kutz is with Bell Laboratories, Lucent Technologies, Holmdel, NJ 07733 USA. He is also with the Program in Applied and Computational Mathematics, Princeton University, Princeton, NJ 08544 USA.

M. Koch is with the Physics Department, Ludwig–Maximilians-University, Munich, Germany.

Publisher Item Identifier S 1077-260X(97)09017-5.

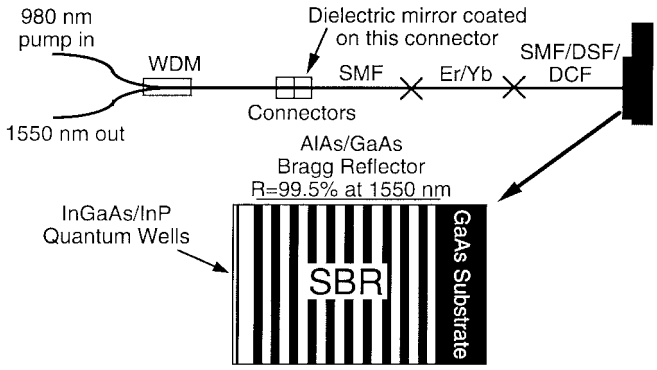

Fig. 1. Schematic of the fiber laser cavity and structure of the SBR.

fiber cavity. Finally, we demonstrate the expansion of the pulse's optical bandwidth to 22 nm by employing SPM. This results in a source suitable for WDM applications with a spectrum covering most of the standard Er-amplifier gain spectrum.

II. General Description of the Erbium Fiber Laser

The linear cavity of this fiber laser consists, in general, of Erbium/Ytterbium (Er/Yb) co-doped single-mode fiber [17] and standard telecommunication single-mode fiber (SMF), (Lucent 5D or Corning SMF-28) spliced in a linear configuration as shown in Fig. 1 [13]. For some cavities, dispersion-shifted fiber (DSF) is spliced into the cavity to increase the cavity length without significantly altering the total cavity dispersion. The length of the Er/Yb fiber is chosen to maximize the saturated gain at wavelengths greater than 1550 nm (typically around 15 cm) and is pumped by a grating stabilized fiber-coupled 90-mW InGaAs diode (SDL BF-SWA0980SDL1190AB) operating near 980 nm. The fiber at one end of the cavity is connectorized with a standard FC connector and a 99% broad-band dielectric output coupler, centered at 1550 nm, is deposited directly onto the polished surface of both the connector ferrule and fiber. This coated connector is coupled with a standard FC coupling sleeve to a second uncoated connector to allow pumping and output coupling through the dielectric coating (>90% transmitting at the pump wavelength). A wavelength division multiplexer separates the output coupled light from the incident pump light as shown in Fig. 1 providing a fiber port for the laser's output. The other end of the fiber cavity is cleaved and butt-coupled to the SBR. The structure of the SBR is shown in Fig. 1 and consists of a Bragg reflector of alternating quarter-wave layers of GaAs and AlAs with two InGaAs–InP quantum wells grown near the surface of a half-wave strain relief layer. The Bragg reflector has a reflection bandwidth of approximately 150 nm centered about 1550 nm and a (saturated) reflectivity exceeding 99.5%.

The SBR and similar quantum well structures have been used to mode-lock several solid state lasers and provide timing stabilization to harmonically mode-locked fiber lasers [11]–[16], [18]–[26]. Mode-locking of a laser by means of a passive saturable absorber requires an intensity dependent temporal response [27]. In the case of the SBR and

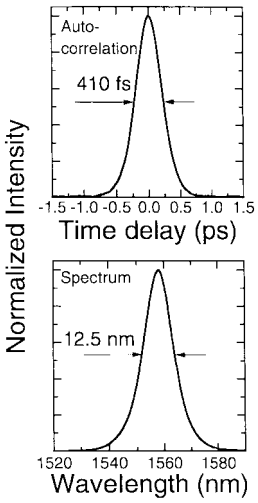

Fig. 2. Typical autocorrelation trace and optical spectrum of the laser output for the anomalous dispersion regime.

other semiconductor saturable absorbers containing quantum wells, both resonant and nonresonant nonlinear absorption effects in the quantum wells can have sufficient ultrafast time responses required to initiate and sustain mode-locking [16], [28]. Resonant absorption effects involve real carrier excitation with recovery times generally greater than 10 ps, causing the quantum well structure to act as a slow saturable absorber. However, intraband carrier–carrier scattering and thermalization processes (i.e., carrier–phonon scattering) can provide a sub-picosecond fast component to the absorption recovery [16]. Near-resonant band edge effects, such as the ac Stark effect, which are nearly instantaneous with the onset of the pulse, can have recovery times of less than 100 fs [28]–[29]. This subpicosecond recovery time of the quantum wells corresponds to an fast increase in the absorption of the quantum wells, and hence, a fast decrease in the reflectivity of the semiconductor structure after the onset of its interaction with the pulse. This mechanism creating an ultrafast temporal window offers the least loss to the shortest pulse [16]. Typically, both resonant and nonresonant effects are present and contribute to the initiation of the mode-locking and the steady-state operation of a laser mode-locked with a SBR or a similar semiconductor saturable element. Fig. 2 shows a typical autocorrelation and optical spectrum of the mode-locked output.

The excitonic absorption of the quantum wells in the SBR designed for the fiber laser presented here is centered around 1540 nm. The fiber laser typically operates at a center wavelength above 1545 nm such that the nonlinear interaction is primarily nonresonant. A pump-probe technique was used to measure the nonlinear reflectivity response of the SBR (10 quantum wells) utilizing 170-fs pulses at several central wavelengths. The ultrafast response is shown in Fig. 3. Note that the $\sim$170 fs fast component of the reflectivity response is approximately the length of the measurement pulse. Furthermore, the shortest fast component occurs at a wavelength of 1550 nm, slightly longer in wavelength than the center of the excitonic absorption. The $\sim$14 ps slow component, caused by the relaxation of excited real

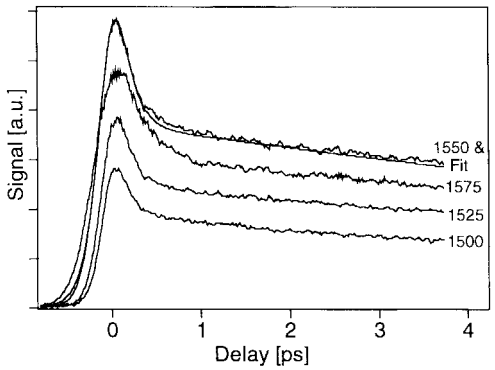

Fig. 3. Pump-probe response of the SBR indicating the relative change in the reflectivity at several wavelengths. The theoretical fit to the response at 1550 nm is superimposed (see Section VI).

carriers, indicates the presence of resonant interactions. The fast (femtosecond) component of the reflectivity, clearly seen in Fig. 3, essentially opens an ultrafast low-loss temporal window and is the mode-locking mechanism offering the least loss to the shortest pulse [16].

Since the cavity consists entirely of optical fiber, both group velocity dispersion and SPM play important roles in pulse shaping [30]. For pulse propagation in a medium of normal dispersion (D $<$ 0 ps/nm/km), the dispersion acts to broaden and chirp the pulse while SPM acts independently, to shape the pulse's optical spectrum. However, in the case of anomalous dispersion (D $>$ 0 ps/nm/km), the two effects can balance each other such that a stable temporal optical soliton is formed [30], [31]. The presence of both dispersion and SPM is a dominant source of pulse shaping effects in a mode-locked laser cavity and must be properly managed for stable operation. Propagation of the fundamental soliton in the anomalous dispersion regime has the desirable properties of stability against small perturbations, production of transform-limited pulses and quantization of the product of the pulse's energy and pulsewidth. This quantization effectively causes the pulse to continuously alter its width and energy attempting to achieve the proper width and energy of a fundamental soliton [32], [33]. For this laser, the Er/Yb gain fiber has a dispersion value of -9 ps/nm/km at 1550 nm and SMF has a value of $+16$ ps/nm/km allowing the sign and magnitude of the total dispersion of the cavity to be varied in both the normal and anomalous regimes simply by changing the relative lengths of each type of fiber used in the cavity. The operation of the laser is very different in the two dispersion regimes and will be discussed both experimentally and theoretically. DSF (approximately zero dispersion) is also used for cavity length variation with minimal alteration of the total cavity dispersion.

To maximize the saturated gain in the Er/Yb fiber for longer wavelengths, the length of the Er/Yb fiber is optimized due to the tradeoff between the gain offered in the front or pumped end of the Er/Yb fiber and the reabsorption in the tail or unpumped region. Due to unequal saturated gain and absorption responses of the fiber versus wavelength, the spectral region of operation is chosen by tailoring this ratio. This is done experimentally by changing the length of the Er/Yb fiber for a given pump intensity and wavelength. For this laser, the Er/Yb fiber length is chosen for operation about 1560 nm, typically between 15 and 20 cm and is determined with a simple cutback method.

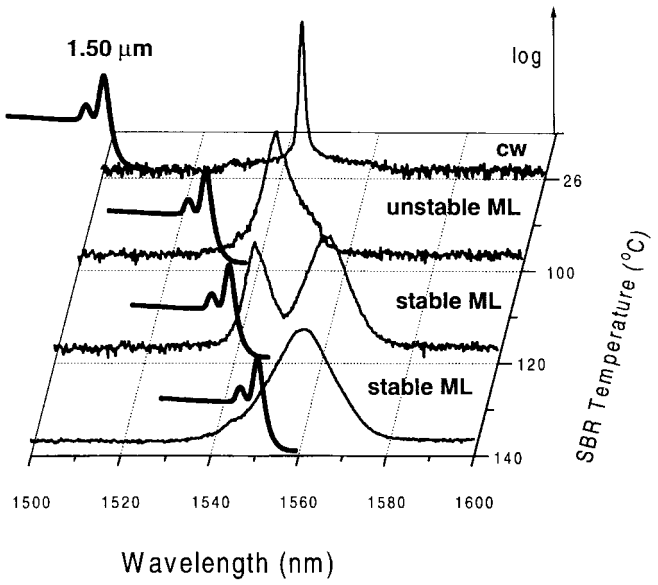

Fig. 4. Optical spectrum (thin line) of laser output and approximate exciton absorption (thick line) for various temperatures of the SBR.

We have designed all of the fiber lasers presented here with telecommunication quality components. In particular, the pump diodes (SDL) have a failure rate of 300 devices in 10^9 device hours. The SBR mode-locking mechanism provides stable mode-locking for low intracavity powers allowing the use of these reliable, low power diode pumps. This is in comparison to fiber lasers utilizing other mode-locking mechanisms with large intracavity losses that require larger intracavity powers, and hence, high-power pump lasers with significantly less reliability.

III. Effect of the Exciton Energy on the Mode-Locking Dynamics

The peak energy of the quantum-well exciton can be tuned by changing the temperature of the sample with an approximate energy shift of 0.4 meV/C. This allows us to vary the interaction between the quantum wells and the laser pulse by moving the exciton wavelength with respect to the optical spectrum. As discussed in Section II, the nonlinear interaction between the pulse and quantum wells occurs through both resonant and nonresonant ultrafast interactions. It is observed that the most stable and shortest pulses are obtained when the center wavelength of the optical spectrum of the pulses is slightly longer than the peak wavelength of the exciton absorption, i.e., the interaction is primarily nonresonant [16].

For this experiment, a SBR with an exciton absorption wavelength centered around 1500 nm was fabricated such that the exciton absorption wavelength could be shifted (with heating) to longer wavelengths toward center of the laser's spectrum. Fig. 4 shows the laser spectrum and approximate exciton absorption for various temperatures of the SBR. In the case where the exciton absorption is well separated from the operating wavelength of the laser ($\sim$26 °C), no mode-locking

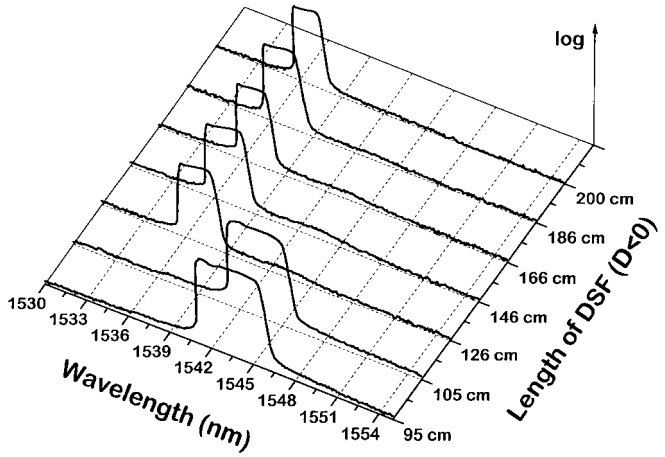

Fig. 5. Optical spectra of the pulses generated with the laser operating in the normal dispersion regime for different lengths of DCF.

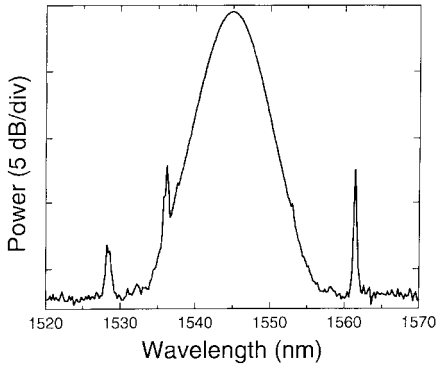

Fig. 6. Optical pulse spectrum of the fiber laser output with resonance sidebands present.

occurs. As the temperature increases, the detuning decreases and the degree of interaction between the pulse and the quantum wells increases. With a smaller amount of interaction (SBR temperature $\sim$26 °C–100 °C), weaker mode-locking produces a narrow and noisy optical spectrum as seen in Fig. 4. The greatest optical bandwidth and stability occurs where the wavelength of the exciton absorption is slightly shorter than the center of the optical spectrum (SBR temperature $\sim$140 °C). Here, the bulk of the optical spectrums just below the exciton absorption and thus, subjected to the nonresonant saturation dynamics of the quantum wells. Since the nonresonant saturable absorption is strongest at wavelengths slightly longer than the peak of the exciton absorption, a pulse with a center wavelength slightly longer than the wavelength of the exciton absorption experiences the most nonlinear saturable absorption [28], [29]. This corresponds to the wavelength separation incurring the strongest mode-locking mechanism. This behavior is supported by the results in Fig. 3, where the shortest and largest relative response occurs at approximately the same detuning of the exciton absorption from the center of the laser spectrum. Note that the center of the exciton absorption for the SBR used in the pump-probe experiment is approximately at the same wavelength as the SBR at $\sim$140 °C in Fig. 3.

IV. Effect of Cavity Dispersion and Length (Experimental)

In this section, we investigate the effect of cavity dispersion on the characteristics of the ultrashort pulses generated with the SBR-mode-locked fiber lasers. We have constructed three cavities with different net dispersions by adding three types of fiber, dispersion compensating fiber (DCF, D $= -51.6$ ps/nm/km), DSF and SMF (D $= +16$ ps/nm/km), to the basic laser cavity shown in Fig. 1.

A. Normal Dispersion Regime

To study the laser's operation in a regime of normal dispersion, we built a cavity with 13 cm of SMF (output coupling end of cavity), 19 cm of Er/Yb fiber and 200 cm of DCF (butt-coupled to SBR). For this cavity, we observe the formation of a very stable pulse train with a square-shaped optical spectrum (see Fig. 5). For 200 cm of DCF, the spectrum is centered around 1535 nm corresponding to the first gain peak of the Er/Yb fiber where the small signal gain is largest. Decreasing the length of the DCF and hence the cavity losses (the loss of the DCF is estimated to be $>$10 dB/km), drives the gain deeper into saturation This tends to shift the spectrum toward longer wavelengths where the saturated gain is larger (although the small signal gain is smaller) as discussed in Section II. With a final DCF length of 95 cm, the average cavity dispersion is -38 ps/nm/km. In this situation, the pulses are measured to be 16 ps [full-width at half-maximum (FWHM)] with a $\sim$40-MHz repetition rate. The output power is 250 μW.

B. Anomalous Dispersion (Soliton) Regime

For operation in the anomalous dispersion regime, the length of the SMF is increased to 26 cm and 160 cm of DSF is added to conserve the total cavity length. The average dispersion is $+2.76$ ps/nm/km and 410-fs pulses are generated (see Fig. 2) at a 50-MHz fundamental repetition rate. The average output power is again 250 μW with 12 nm of optical bandwidth centered about 1560 nm (shown in Fig. 2). The time–bandwidth product is 0.62, (twice the transform limited value assuming a sech^2 pulseshape) indicating that the pulses are not transform-limited.

Eliminating the DSF from the cavity, the laser operates at a 200-MHz fundamental repetition rate with an average cavity dispersion of $+5.3$ ps/nm/km. The pulse characteristics are unchanged and the optical spectrum displays no resonant sidebands. However, replacement of the DSF with 150 cm of SMF increases the average cavity dispersion to $+14.1$ ps/nm/km and sidebands emerge in the spectrum symmetric about the peak (see Fig. 6). As in other fiber lasers operating with comparably high anomalous cavity dispersion, sidebands are produced by periodic perturbations to the pulse which lead to coherent shedding of light into a nonsoliton CW background [34]. As verified in this fiber laser cavity, the presence of the sidebands can be avoided by reducing the average cavity dispersion and size of dispersion perturbations.

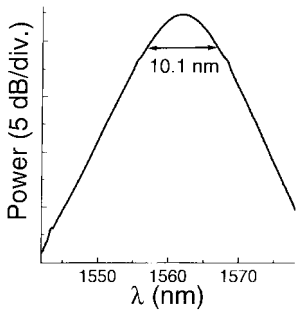

Fig. 7. Optical spectrum of the laser operating at 155 MHz. The FWHM is indicated.

V. Higher Fundamental Repetition Rates

High-repetition rates are a requirement for many potential applications of mode-locked lasers. This is particularly true in optical communications where the repetition rate typically determines the data rate [1].

Using active harmonic mode-locking, it is possible to achieve high-repetition rates. However, with active mode-locking alone, it is very difficult to obtain subpicosecond operation. Several designs have, therefore, incorporated both active mode-locking and passive pulseshaping [33], [35]–[38]. Additionally, supermode competition in harmonically mode-locked lasers can result in noisy, unstable pulse trains. Consequently, additional stabilization techniques must often be employed [36], [37]. In the laser described here, stable passive harmonic mode-locking has been observed (see Section VIII), although the mechanisms causing the stable operation are not currently completely understood.

It is also advantageous to be able to operate at repetition rates that match standard communications bit rates. Hence, we have built a mode-locked fiber laser that operates at a repetition rate of 155.4 MHz (the OC-3 standard is 155.52 MHz). The basic laser design is the same as described in Section II, with three sections of fiber and a net cavity length of 65.7 cm. The first and third sections of standard SMF are approximately equal in length and the center section is 20 cm of Er/Yb fiber. With careful trimming of the fiber cavity length, it is possible to tune the repetition rate to within 200 kHz (mm tolerance in the length). The laser is pumped at 983 nm by a 90 mW diode, however, only 35–40 mW of pump power are typically used. Multiple pulsing occurs at higher pump powers and a smaller optical bandwidth is produced at lower pump powers. At an optimal pumping level, this laser produces 150 μW of output power with a bandwidth of 10.1 nm centered about 1561 nm (see Fig. 7). This laser is self-starting and with proper mechanical design, stable for long periods of time.

It is desirable to achieve even higher fundamental repetition rates. There are two factors that provide a practical upper limit on the repetition rate. The first is simply the length of gain fiber required to provide sufficient gain to overcome cavity losses, which are independent of cavity length (output coupling, SBR coupling and splices). We find that approximately 10 cm of Er/Yb fiber is necessary to overcome these losses in the current design. The other factor is the need to maintain net anomalous dispersion in the cavity as soliton pulse shaping is crucial for obtaining subpicosecond pulses (see Sections IV and VI). Since the gain fiber has normal dispersion (-9 ps/nm/km), it is typically necessary to have approximately twice as much standard fiber ($+16$ ps/nm/km) as gain fiber. These factors limit the fundamental repetition rate to around 300 MHz for the current design.

For many applications it is necessary to lock the repetition frequency of the laser to an external reference in addition to synchronizing the phase of the output pulse train with that of the reference. By using a combination of a piezoelectric fiber stretcher and a heater wire coiled around the fiber of a section of the laser cavity correcting for fast and slow cavity length variations, respectively, we have managed to synchronize a fiber laser with an external reference for time periods longer than 24 h. Synchronization with timing jitter of 40 ps or less has been achieved in lower repetition rate mode-locked fiber lasers of different designs [39].

VI. Analytic and Numerical Model of the Mode-Locking Dynamics

In this section, we highlight the modeling issues important for an analytic understanding of the laser mode-locking dynamics. We describe a model that couples an accurate description of the pulse dynamics in the fiber with a phenomenological description of the SBR dynamics predicting results quantitatively consistent with the experimentally observed behavior. We begin by considering a propagating pulse in a laser cavity under the influence of the Kerr nonlinearity, dispersion, loss, and a parabolic gain bandwidth and which is governed by the modified nonlinear Schrödinger equation (Ginzburg–Landau equation) [40], [41]:

$$i\frac{\partial Q}{\partial Z}+\frac{\lambda_0^2\overline{D}}{4\pi c}\frac{\partial^2 Q}{\partial T^2}+\frac{2\pi n_2}{\lambda_0 A_{\text{eff}}}|Q|^2Q+i\Gamma Q-iG(Z)\cdot\left(1+\frac{1}{\Omega^2}\frac{\partial^2}{\partial T^2}\right)Q=0. \quad (1)$$

Here, Q is the electric field envelope, T is the physical time in the rest frame of the pulse and Z is the propagation distance. The Kerr coefficient of the fiber is taken to be $n_2 = 2.6 \times 10^{-16}$ cm^2/W, the effective cross-sectional area $A_{\text{eff}} = 60$ μm^2, and $\Gamma = 0.0230$ km^{-1} which corresponds to a power loss of 0.20 dB/km. $\overline{D}$ is the average cavity dispersion (in ps/km/nm), Ω is the gain bandwidth of the fiber, and $\lambda_0 =$ 1550 nm and c are the vacuum wavelength and speed of light, respectively.

The gain in the fiber is incorporated through the parameter $G = G(Z)$. We model the saturated gain in the fiber by setting [40]

$$G(Z)=\frac{2G_0}{1+\|Q(Z)\|^2/E_{\text{sat}}} \quad (2)$$

where E_{sat} is the saturation energy of the fiber, G_0 is the saturated gain, and $\|Q(Z)\|^2 = \int_{-\infty}^{\infty}|Q(Z)|^2dT$ is the pulse energy.

The mode-locking action of the SBR is incorporated via an empirical model of its nonlinear temporal response (discussed in Section II). The reflectivity response of the SBR is treated as a jump condition to the propagation (1) and includes a "fast"

component representative of the nonresonant interactions and a "slow" component, representative of the real transitions [14], [16], [28]. The combined response can be described by the jump condition [40]

$$Q_+ = \left(1 - \sigma_l - \sigma_f \left[1 - \frac{|Q_-|^2}{|Q_-|^2_{\max}} \right] - \sigma_s \left\{ 1 - \frac{\int_{-\infty}^{T} |Q_-|^2 \, dT}{\|Q_-\|^2} \cdot \exp \left[-H(T - T_{\max}) \frac{T - T_{\max}}{T_d} \right] \right\} \right) Q_- \quad (3)$$

where $Q_\pm$ denotes the pulse before $(-)$ and after $(+)$ interaction with the SBR, T_d is the decay time of the SBR slow response, σ_l is the intrinsic loss of the SBR, σ_f measures the relative strength of the instantaneous SBR response and σ_s is the relative strength of the corresponding slow saturation response. Note that $|Q(T_{\max})| = |Q|_{\max}$ gives the power maximum and its relative position, and $H(T - T_{\max})$ is the standard Heaviside function for which $H(T - T_{\max}) = 0$ for $T - T_{\max} < 0$ and $H(T - T_{\max}) = 1$ for $T - T_{\max} > 0$. The jump condition (3) is a phenomenological idealization of the interaction dynamics of the SBR with the electric field near steady-state mode-locking [40]. In Fig. 3, we compare this simple SBR model with pump-probe measurements assuming a hyperbolic secant pulse in (3), $T_d = 14$ ps, $\sigma_l = 0.005$ for a saturated reflectivity of 99.5%, and $\sigma_f = \sigma_s = 0.65\,\sigma$ where σ is the maximum change in reflectivity of the SBR. We estimate from experiments that the maximum change in reflectivity is $\approx$2% so that $\sigma = 2\%$ and $\sigma_f = \sigma_s = 1.3\%$.

Finally, the output coupler can be similarly incorporated into the numerical model by simply implementing the appropriate jump condition

$$Q_+ = RQ_- \quad (4)$$

where R is the reflectivity of the output coupler.

Equations (1)–(4) provide a numerical model capable of describing the mode-locking dynamics. We can extend this model by incorporating the effects of the SBR and output coupler into the evolution (1) by an appropriate averaging procedure [40]. This leads to the averaged evolution equation:

$$i\frac{\partial Q}{\partial Z} + \left[\frac{\lambda_0^2 \overline{D}}{4\pi c} - i\frac{G(Z)}{\Omega^2} \right] \frac{\partial^2 Q}{\partial T^2} + \left(\frac{2\pi n_2}{\lambda_0 A_{\text{eff}}} - i\frac{\sigma_f}{|Q|^2_{\max}} \right) \cdot |Q|^2 Q + i[\gamma - G(Z)]Q - i\sigma_s \frac{\int_{-\infty}^{T} |Q|^2 \, \mathrm{d}T}{\|Q\|^2} \cdot \exp \left[-H(T - T_{\max}) \frac{T - T_{\max}}{T_d} \right] Q = 0 \quad (5)$$

where $\gamma = \Gamma + 1 - R + \sigma_l + \sigma_f + \sigma_s$. Equation (5) is the analog of Haus' master mode-locking model [41] with some significant differences due to the normalization of the instantaneous response and the addition of the slow response. In the case where the SBR has no slow response, i.e., $\sigma_s = 0$, (5) admits an exact solution of the form [40]

$$Q(Z, T) = \eta[\operatorname{sech}(\omega T)]^{1+iA} \exp[i\phi(Z)] \quad (6)$$

where the parameters A, η, ω, and $d\phi/dz$ are determined from a system of nonlinear algebraic equations.

In the numerical simulations that follow, $\sigma_s = 1.3\% \neq 0$. Thus, special care must be taken to incorporate the effective contribution of the slow response to the parameters of (6) [40]. We test the above models by considering the mode-locking dynamics in the normal dispersion regime. For this case, the experimental laser cavity consists of 19 cm of Er/Yb fiber, 13 cm of SMF and 95 cm of DCF giving an average cavity dispersion of $\overline{D} \approx -38$ ps/km/nm and a saturated intracavity power measured experimentally at $E_{\text{sat}} = 21.3$ mW. We assume the fiber has a 25-nm gain bandwidth and take the initial energy to be half the saturated energy of the cavity. In Fig. 8, we compare experimental pulse profiles and optical spectra with the steady-state (numerical) solutions of the full governing equations (1)–(4), the averaged evolution (2) and (5), and the analytic solution (6).

Similarly, we consider the case for which the average dispersion in the fiber cavity is in the anomalous regime. In

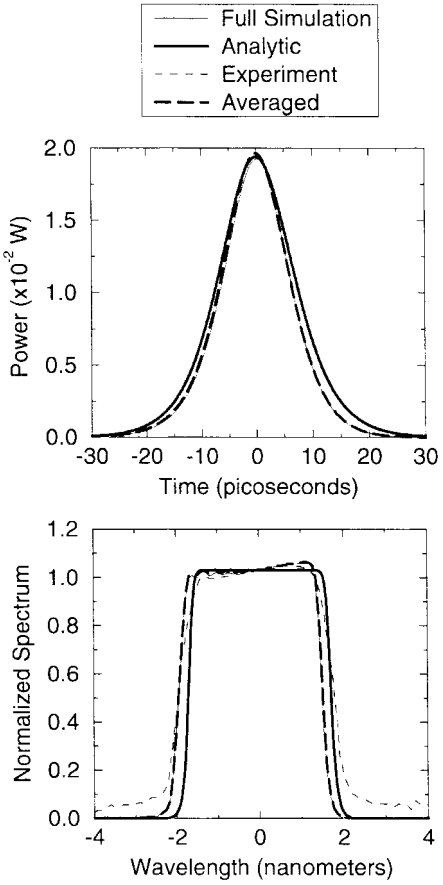

Fig. 8. Steady-state pulse profiles and optical spectra given by (1)–(4) and comparison of this model with the averaged model, the analytic approximation and the experimental findings.

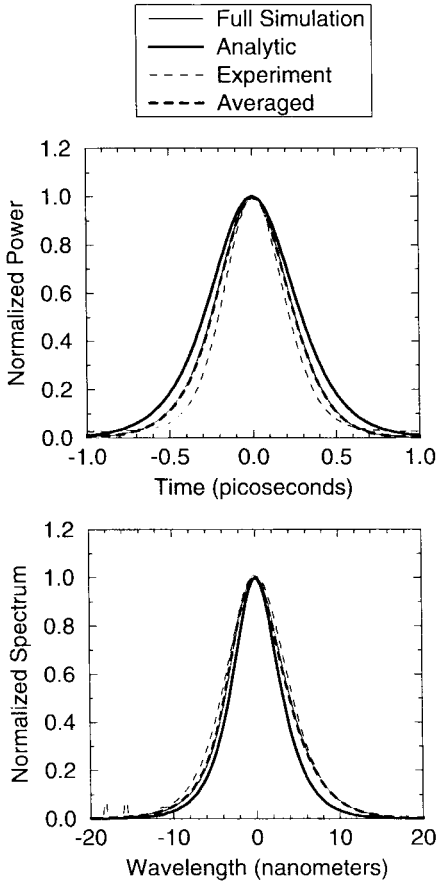

Fig. 9. Steady-state pulse profiles and optical spectra given by (1)–(4) and comparison of this model with the averaged model, the analytic approximation and the experimental findings.

this case, the cavity consists of 17 cm of Er/Yb fiber and 24- and 49-cm sections of SMF giving an average dispersion value of $\overline{D} \approx 12$ ps/km/nm. The output coupling is 2% and the intracavity power is estimated from measurements to be $\approx$10 mW. We take an artificially large gain bandwidth of $\approx$45 nm. This is needed since the gain profile is considerably flatter than the parabolic shape assumed in the model. The steady-state bandwidth is a result of the interplay between the broadening and restriction of the bandwidth, due to the SPM and gain, respectively. The validity of the proposed evolution model is again tested by comparing predictions directly to experimental results. In Fig. 9, we compare the predictions of the model with experimental output profiles for the anomalous dispersion case in the manner of Fig. 8.

The comparisons between theory and experiment show that the model provides a quantitatively accurate method for exploring the mode-locking dynamics. Furthermore, it elucidates the essential role of the nonresonant temporal response in driving the mode-locking. A comprehensive treatment of the above model and associated dynamics can be found in Kutz *et al.* [40].

VII. Nonlinear Spectral Broadening

Many applications require a broader spectrum than can be obtained directly from the fiber lasers described here. For example, a source for a communications system should fill

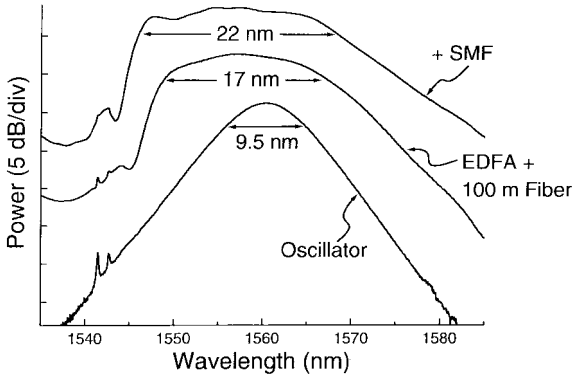

Fig. 10. Optical spectra from bottom to top: output of oscillator, after amplifier and 100 m of low normal dispersion fiber and after further propagation through SMF fiber. Spectra are offset vertically for clarity.

the gain bandwidth of standard erbium amplifiers ($\sim$25 nm). For all lasers presented here, output bandwidths greater than 12 nm could not be produced. To achieve a larger bandwidth, we amplify the oscillator output and launch it into fiber of low normal dispersion. The resulting SPM of the short pulse in the low-dispersion fiber produces spectral broadening. This is similar to supercontinuum generation [42], which has been used to obtain a broad spectrum from mode-locked fiber lasers. However, by using shorter pulses and lower average powers so that SPM is the dominant nonlinear process, we obtain a stable output spectrum that is relatively flat over the region of interest. Nonlinear spectral broadening is less stable for larger broadening ratios (final to initial bandwidth). As we are only increasing the spectral width by approximately a factor of 2, we obtain a very stable output spectrum, whereas the results for supercontinuum generation are less stable due to the large broadening ratio. Supercontinuum generation tends to have greater spectral structure due to the increased significance of additional nonlinear effects.

To obtain a high enough intensity so that significant broadening is produced, the output of the oscillator is amplified in an erbium fiber amplifier consisting of 28 m of erbium doped gain fiber [43], forward pumped by a 90-mW diode (SDL). An output power of 8.7 mW is obtained for an input of 120 μW. Because the gain fiber has large normal dispersion, it is necessary to precompensate for this dispersion by passing the pulses through 130 m of SMF before the amplifier. This results in an output pulse with a small anomalous chirp. The pulse then undergoes compression and SPM in 100 m of fiber with small normal dispersion near 1550 nm ($\lambda_0 = 1575$ nm), producing spectral broadening from an input FWHM of 9.5 to 17 nm at the output (see Fig. 10). At this point, the pulse has a small normal chirp, such that launching it into SMF causes temporal recompression and additional SPM, yielding a final spectral width of 22 nm.

VIII. Passive Harmonic Mode-Locking

The quantization of the cavity energy into fundamental solitons provides a passive method for controlling the number of pulses circulating in the cavity by adjustment of the energy in the cavity [44]. Limits on the pulsewidth arising from

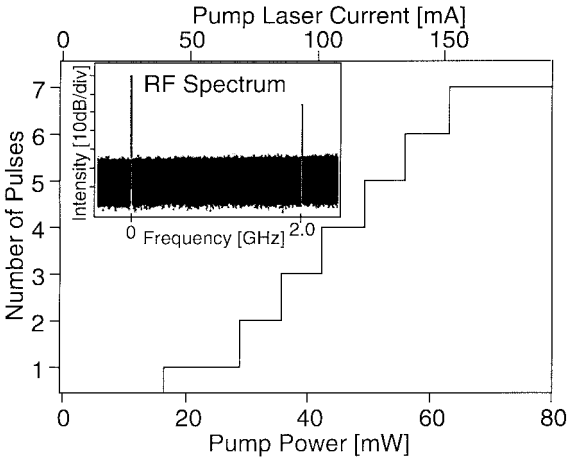

Fig. 11. Number of circulating pulses versus pump power. Inset: RF spectrum of the laser output operating at 2.06 GHz indicating the suppression of lower cavity harmonics by over 30 dB.

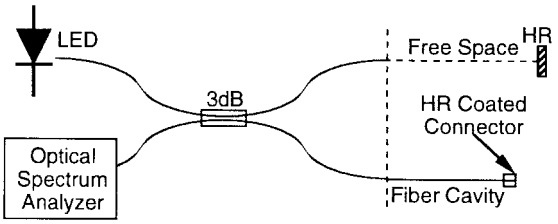

Fig. 12. Schematic of the Michelson interferometer used to measure cavity dispersion.

the available gain bandwidth or mode-locking mechanism are important for determining the number of pulses in the cavity. Without these constraints, increasing the energy in a single fundamental soliton would simply decrease the pulsewidth according to standard soliton theory [30]. However, the finite gain bandwidth puts a lower bound on the pulsewidth by limiting the optical bandwidth. Likewise, the mode-locking mechanism which offers less loss to a shorter pulse creates a "soft" upper bound on the pulsewidth. For these reasons, multiple pulsing occurs, in general, for cases where the cavity energy is greater than twice the energy of the gain bandwidth-limited single fundamental soliton pulse. Due to the strong soliton pulse shaping effects determined by the cavity, all pulses in the cavity are typically of the same energy and pulsewidth. Equal spacing of the pulses is believed to be the result of gain saturation dynamics.

For achieving higher repetition rates, a cavity consisting of a single span of 22.3 cm SMF and 12.5 cm Er/Yb fiber was constructed with a 290-MHz fundamental repetition rate. The Er/Yb fiber was butt-coupled to the SBR. Harmonic mode-locking was observed with up to seven equally spaced pulses in this cavity resulting in a repetition rate of 2.1 GHz. Fig. 11 gives the RF spectrum of the output measured with a fast photodiode, showing at least 30 dB suppression of lower cavity harmonics. The pulsewidth is about 350 fs with 11 nm of optical bandwidth. Decreasing the pump power causes a systematic decrease in the number of pulses in accordance with the energy quantization provided by the soliton dynamics as illustrated in Fig. 11. The most stable harmonic mode-locking and correspondingly best suppression of lower cavity harmonics in the RF spectrum typically occurs near the midpoint of the pump current necessary to sustain a given number of pulses, consistent with behavior observed in similar passive systems [26]. Unlike harmonically mode-locked fiber lasers with considerably lower fundamental repetition rates ($<$20 MHz), where on the order of 100 pulses are necessary to achieve a 2-GHz repetition rate [25], [45], small pump fluctuations do not lead to changes in the number of pulses due to the large ratio of the single-pulse energy to the total cavity energy.

Timing jitter in passive harmonically mode-locked lasers arises from additional sources, relative to nonharmonically mode-locked lasers, due to the ability of the multiple pulses to randomly walk in time with respect to each other. Similar to a soliton transmission line, timing jitter occurs due to the Gordon–Haus effect [46]. The Gordon–Haus timing jitter is caused by periodic amplitude fluctuations, that when coupled with propagation in media of differing dispersion, contribute to timing shifts. The excitation of acoustic modes of the fiber by the solitons leads to index fluctuations which also contribute further phase noise and timing jitter [47]–[49]. The temporal jitter of the laser operating at 2.1 GHz was measured by analysis of the RF spectrum of the laser's output [50] and found to be less than 1.5 ps over a 1-kHz frequency range. Subpicosecond jitter has been reported in other passive harmonically mode-locked lasers and mechanisms such as soliton–soliton interactions due to the acoustic effect and phase modulation occurring in a semiconductor saturable absorber are believed to be stabilizing effects [25], [26]. Recently, Grudinin suggested that fluctuations in the cavity length can provide effective phase modulation, reducing the temporal jitter [45]. The mechanism producing the reduced temporal jitter in this laser is currently under investigation. Since the slow recovery of the SBR used in this fiber laser has been measured to be 14 ps, phase modulation in the SBR is not believed to be significant.

IX. Conclusion

We have presented short cavity passively mode-locked Er/Yb fiber lasers and have investigated the mechanisms governing their operation. We have included a theoretical model that quantitatively predicts the steady-state mode-locked laser output for both normal and anomalous dispersion regimes and have demonstrated harmonic operation resulting in a 2-GHz repetition rate.

Appendix
Technique for Measuring the Total Cavity Dispersion

Measurement of the total cavity dispersion is useful since the dispersion of the high loss Er/Yb fiber cannot be measured by a conventional time-of-flight technique. We have also found that in a short ($<$1 m) piece of standard fiber, the dispersion can differ significantly from the average value obtained with a measurement of the entire several kilometer spool. This

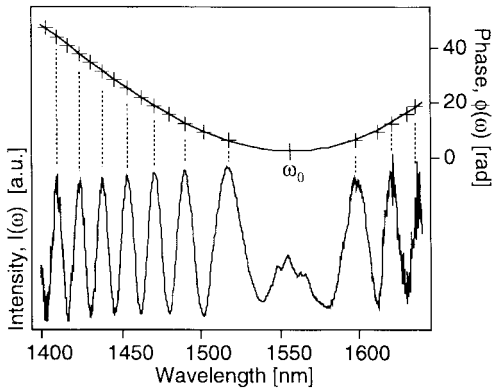

Fig. 13. Typical normalized optical spectrum measured out one port of the interferometer is shown in the bottom curve. The plot of the associated phase (crosses) created by locating each peak and valley of the normalized spectrum and assigning the proper phase value is shown The fit of the theory used to determine β_2 is superimposed (solid line).

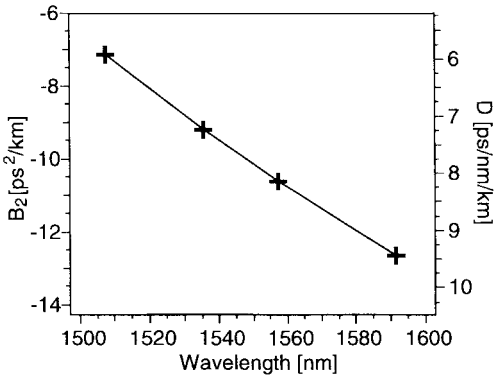

Fig. 14. Measured total dispersion versus wavelength for a typical fiber cavity.

technique described here uses a balanced Michelson interferometer illuminated with a broad-band source and allows the measurement of the total dispersion in a complete fiber laser cavity (see Fig. 12) [51]–[53]. One arm of the interferometer is free space and the other is the laser cavity under test. Both arms are terminated with a broad-band mirror. Injecting light into one port of the interferometer, the intensity at the other port can be written

$$I(\omega) = |E_{\rm fs}(\omega) + E_{\rm f}(\omega)|^2 \approx 1 - \cos[\phi(\omega)] \tag{7}$$

$$\phi(\omega) = \beta_{\rm fs}(\omega)d - \beta_f(\omega)L \tag{8}$$

where $E_{\rm fs}, E_{\rm f}, \beta_{\rm fs}$, and $\beta_{\rm f}$ represent the respective electric fields and propagation constants along the free space and fiber arms, ω is the optical angular frequency, and d and L are the respective lengths of the free space and fiber arms. Expanding $\beta_{\rm f}$ about $\omega_0, \phi(\omega)$ becomes

$$\begin{aligned}\phi(\omega) = \phi_0 &+ \left[\beta_1(\omega_0)L - \frac{d}{c}\right](\omega - \omega_0) \\ &+ \tfrac{1}{2}\beta_2(\omega_0)L(\omega - \omega_0)^2 \\ &+ \tfrac{1}{6}\beta_3(\omega_0)L(\omega - \omega_0)^3 + \cdots\end{aligned} \tag{9}$$

where ϕ_0 is a constant, c is the speed of light in vacuum, β_2 is the total group velocity dispersion and β_3 is the third order dispersion of the fiber cavity. By adjusting the length of the free space arm such that $\beta_1(\omega_0)L = d/c$, the phase difference between $E_{\rm fs}$ and $E_{\rm f}$ is reduced to terms of second order and higher in the frequency difference. The spectrum of the light at the output port contains nulls at frequencies where $\phi(\omega) = 2n\pi$ (n is an integer) and peaks where $\phi(\omega) = 2\pi(n+1)$ as shown in Fig. 13.

The experimental setup is shown in Fig. 12. A 3-dB fiber coupler serves as a beam splitter with the fiber pigtails of both interferometer arms cut equal to approximately a 1-mm tolerance in order to avoid any dispersive contribution from the pigtail fibers. This assumes equal amounts of dispersion in both fiber pigtails, which was measured to be the case. The bare fiber end of the cavity is spliced to one of the fiber pigtails and the output of the other pigtail is collimated and propagated through a variable length free space region approximately equivalent to the optical length of the fiber cavity. A fiber coupled broad-band LED (60-nm FWHM centered at 1515 nm, MRV Technologies) producing 30 μW is injected into one port of the 3-dB coupler and the output of the other port is monitored with a high dynamic range optical spectrum analyzer. Normalization of the light from the output port with respect to the spectrum of the LED gives a typical pattern shown in Fig. 13. The magnitudes of β_2 and β_3 at ω_0 are found by determining the optical frequency in which each peak and valley occurs, constructing the corresponding phase difference versus frequency plot (Fig. 13) and fitting the measured phase difference to $\phi(\omega)$. Measuring the delay of the free space arm at each ω_o and determining the sign of the slope of this delay with respect to optical frequency gives the sign of β_2. Figs. 13 and 14 include a typical fit and measurement results of a 270-MHz cavity. The error in β_2 is estimated to be ± 0.05 ps^2/km.

REFERENCES

[1] M. C. Nuss, W. H. Knox, and U. Koren, "Scalable 32 channel chirped-pulse WDM source," *Electron. Lett.*, vol. 32, pp. 1311–1312, 1996.
[2] I. N. Duling, III, and M. L. Dennis, *Compact Sources of Ultrashort Pulses.* Cambridge, U.K.: Cambridge Univ. Press, 1995.
[3] H. A. Haus, J. G. Fujimoto, and E. P. Ippen, "Analytic theory of additive pulse modelocking and Kerr lens modelocking," *IEEE J. Quantum Electron.*, vol. 28, pp. 2086–2096, 1992.
[4] K. Tamura, H. A. Haus, and E. P. Ippen, "Self-starting additive pulse modelocked erbium fiber ring laser," *Electron. Lett.*, vol. 28, pp. 2226–2227, 1992.
[5] H. A. Haus, E. P. Ippen, and K. Tamura, "Additive pulse modelocking in fiber lasers," *IEEE J. Quantum Electron.*, vol. 30, pp. 200–208, 1994.
[6] I. N. Duling, III, "Subpicosecond all-fiber erbium laser," *Electron. Lett.*, vol. 27, pp. 544–545, 1991.
[7] D. J. Richardson, R. I. Laming, D. N. Payne, V. J. Matsas, and M. W. Phillips, "Selfstarting, passively modelocked erbium fiber laser based on the amplifying Sagnac switch," *Electron. Lett.*, vol. 27, pp. 542–543, 1991.
[8] M. L. Dennis and I. N. Duling, III, "High repetition rate figure eight laser with extracavity feedback," *Electron. Lett.*, vol. 28, pp. 1894–1896, 1992.
[9] M. E. Fermann, M. J. Andrejco, Y. Silverberg, and M. L. Stock, "Passive modelocking by using nonlinear polarization evolution in a polarizing-maintaining erbium-doped fiber," *Opt. Lett.*, vol. 18, pp. 894–896, 1993.
[10] H. A. Haus and A. Mecozzi, "Noise in mode-locked lasers," *IEEE J. Quantum Electron.*, vol. 29, pp. 983–996, 1993.

[11] E. A. De Souza, C. E. Soccolich, W. Pleibel, R. H. Stolen, J. R. Simpson, and D. J. DiGiovanni, "Saturable absorber modelocked polarization maintaining erbium-doped fiber laser," *Electron. Lett.*, vol. 29, pp. 447–449, 1993.
[12] W. H. Loh, D. Atkinson, P. R. Morkel, M. Hopkinson, A. Rivers, A. J. Seeds, and D. N. Payne, "Passively mode-locked Er^{3+} fiber laser using a semiconductor nonlinear mirror," *IEEE Photon. Technol. Lett.*, vol. 5, pp. 35–37, 1993.
[13] S. Tsuda, W. H. Knox, J. L. Zyskind, J. E. Cunningham, W. Y. Jan, and R. Pathak, "Broadband compact mode-locked Er/Yb:fiber laser," presented at the Conf. Laser and Electro-Optics, Anaheim, CA, 1996, paper CFD2.
[14] S. Tsuda, W. H. Knox, E. A. de Souza, W. Y. Jan, and J. E. Cunningham, "Low-loss intracavity AlAs/AlGaAs saturable Bragg reflector for femtosecond modelocking in solid-state lasers," *Opt. Lett.*, vol. 20, pp. 1406–1408, 1995.
[15] B. C. Collings, J. B. Stark, S. Tsuda, W. H. Knox, J. E. Cunningham, W. Y. Jan, R. Pathak, and K. Bergman, "Saturable Bragg reflector self-starting passive mode locking of a Cr^{4+}:YAG laser pumped with a diode-pumped Nd:YVO_4 laser," *Opt. Lett.*, vol. 21, pp. 1171–1174, 1996.
[16] S. Tsuda, W. H. Knox, S. T. Cundiff, W. Y. Jan, and J. E. Cunningham, "Modelocking ultrafast solid-state lasers with saturable Bragg reflectors," *IEEE J. Select. Topics Quantum Electron.*, vol. 2, pp. 454–464, Sept. 1996.
[17] Lucent Technologies Er/Yb co-doped fiber, Comcode 107770927.
[18] U. Keller, D. A. B. Miller, G. D. Boyd, T. H. Chiu, J. F. Ferguson, and M. T. Asom, "Solid-state low-loss intracavity saturable absorber for Nd:YLF lasers: An antiresonant semiconductor Fabry–Perot saturable absorber," *Opt. Lett.*, vol. 17, pp. 505–507, 1992.
[19] U. Keller, T. H. Chiu, and J. F. Ferguson, "Self-starting femtosecond mode-locked Nd:glass laser that uses intracavity saturable absorbers," *Opt. Lett.*, vol. 18, pp. 1077–1079, 1993.
[20] F. X. Kärtner, L. R. Brovelli, D. Kopf, M. Kamp, I. Calasso, and U. Keller, "Control of solid-state laser dynamics by semiconductor devices," *Opt. Eng.*, vol. 34, pp. 2024–2036, 1995.
[21] N. H. Rizvi, P. M. French, J. R. Taylor, P. J. Delfyett, and L. T. Florez, "Generation of pulses as short as 93 fs from self-starting femtosecond Cr:$LiSrAlF_6$ laser by exploiting multiple-quantum well absorbers," *Opt. Lett.*, vol. 18, pp. 983–985, 1993.
[22] L. R. Brovelli, I. D. Jung, D. Kopf, M. Kamp, M. Moser, F. X. Kärtner, and U. Keller, "Self-starting soliton modelocked Ti–sapphire laser using a thin semiconductor saturable absorber," *Electron. Lett.*, vol. 31, pp. 287–288, 1995.
[23] R. Fluck, G. Zhang, U. Keller, K. J. Weingarten, and M. Moser, "Diode-pumped passively mode-locked 1.3 μm Nd:YVO_4 and Nd:YLF lasers by use of a semiconductor saturable absorbers," *Opt. Lett.*, vol. 21, pp. 1378–1380, 1996.
[24] C. Hönninger, G. Zhang, U. Keller, and A. Giesen, "Femtosecond Yb:YAG laser using semiconductor saturable absorbers," *Opt. Lett.*, vol. 20, pp. 2402–2404, 1996.
[25] S. Gray and A. B. Grudinin, "Soliton fiber laser with a hybrid saturable absorber," *Opt. Lett.*, vol. 21, pp. 207–209, 1996.
[26] M. E. Fermann and J. D. Minelly, "Cladding-pumped passive harmonically mode-locked fiber laser," *Opt. Lett.*, vol. 21, pp. 970–972, 1996.
[27] H. A. Haus, "Theory of mode locking with a slow saturable absorber," *IEEE J. Quantum Electron.*, vol. QE-11, pp. 735–747, 1975.
[28] D. S. Chemla, W. H. Knox, D. A. B. Miller, S. Schmitt-Rink, J. B. Stark, and R. Zimmermann, "The excitonic optical Stark effect in semiconductor quantum wells probed with femtosecond optical pulses," *J. Luminescence*, vol. 44, pp. 233–246, 1989.
[29] W. H. Knox, D. S. Chemla, D. A. B. Miller, J. B. Stark, and S. Schmitt-Rink, "Femtosecond ac Stark effect in semiconductor quantum well: Extreme low- and high-intensity limits," *Phys. Rev. Lett.*, vol. 62, pp. 1189–1192, 1989.
[30] G. P. Agrawal, *Nonlinear Fiber Optics*, 2nd ed. San Diego, CA: Academic, 1995.
[31] L. F. Mollenauer, R. H. Stolen, and J. P. Gordon, "Experimental observation of picosecond pulse narrowing and solitons in optical fibers," *Phys. Rev. Lett.*, vol. 45, pp. 1095–1098, 1980.
[32] J. D. Kafka, T. Baer, and D. W. Hall, "Mode-locked erbium-doped fiber laser with soliton pulse shaping," *Opt. Lett.*, vol. 14, pp. 1269–1271, 1989.
[33] T. F. Carruthers and I. N. Duling, "10-GHz, 1.3-ps erbium fiber laser employing soliton pulse shortening," *Opt. Lett.*, vol. 21, pp. 1927–1929, 1996.
[34] S. M. J. Kelly, "Characteristic sideband instability of periodically amplified average soliton," *Electron. Lett.*, vol. 28, pp. 806–807, 1992.
[35] R. P. Davey, N. Langford, and A. I. Ferguson, "Subpicosecond pulse generation from erbium doped fiber laser," *Electron. Lett.*, vol. 27, pp. 726–728, 1991.
[36] G. T. Harvey and L. F. Mollenauer, "Harmonically mode-locked fiber ring laser with an internal Fabry–Perot stabilizer for soliton transmission," *Opt. Lett.*, vol. 18, pp. 107–109, 1993.
[37] X. Shan and D. M. Spirit, "Novel method to suppress noise in harmonically modelocked erbium fiber lasers," *Electron. Lett.*, vol. 29, pp. 979–981, 1993.
[38] T. F. Carruthers, I. N. Duling, and M. L. Dennis, "Active–passive modelocking in a single-polarization erbium fiber laser," *Electron. Lett.*, vol. 30, pp. 1051–1053, 1994.
[39] G. Sucha and D. Harter, IMRA America, Inc., personal communication; also, H. Lin, Calmar Optcom, Inc., personal communication.
[40] J. N. Kutz, B. C. Collings, K. Bergman, S. Tsuda, S. Cundiff, W. H. Knox, P. Holmes, and M. I. Weinstein, "Modelocking pulse dynamics in a fiber laser with a saturable Bragg reflector," *J. Opt. Soc. Amer. B*, vol. 14, pp. 2681–2690, 1997.
[41] H. A. Haus, J. G. Fujimoto, and E. P. Ippen, "Structures for additive pulse mode locking," *J. Opt. Soc. Amer. B*, vol. 8, pp. 2068–2076, 1991.
[42] T. Morioka, K. Mori, and M. Saruwatari, "More than 100-wavelength-channel picosecond optical pulse generation from single laser source using supercontinuum in optical fibers," *Electron. Lett.*, vol. 29, pp. 862–864, 1993; T. Morioka, H. Kawanishi, H. Takara, and O. Kamatani, "Penalty-free, 100 Gbit/s optical transmission of <2 ps supercontinuum transform limited pulses over 40 km," *Electron. Lett.*, vol. 31, pp. 124–125, 1995.
[43] Lucent Technologies HE980, Comcode 107528366.
[44] A. B. Grudinin, D. J. Richardson, and D. N. Payne, "Energy quantization in figure eight fiber lasers," *Electron. Lett.*, vol. 28, pp. 67–68, 1992.
[45] A. B. Grudinin and S. Gray, "Passive harmonic mode locking in soliton fiber lasers," *J. Opt. Soc. Amer. B*, vol. 14, pp. 114–154, 1997.
[46] J. P. Gordon and H. A. Haus, "Random walk of coherently amplified solitons in optical fiber transmission," *Opt. Lett.*, vol. 11, pp. 665–667, 1986.
[47] A. B. Grudinin, D. J. Richardson, and D. N. Payne, "Passive harmonic modelocking of a fiber soliton ring laser," *Electron. Lett.*, vol. 29, pp. 1860–1861, 1993.
[48] A. N. Pilipetskii, E. A. Golovchenko, and C. R. Manyuk, "Acoustic effect in passively mode-locked fiber ring laser," *Opt. Lett.*, vol. 20, pp. 907–909, 1995.
[49] E. M. Dianov, A. V. Luchnikov, A. M. Pilipetskii, and A. N. Starodumov, "Electrostriction mechanism of soliton interaction in optical fibers," *Opt. Lett.*, vol. 15, pp. 314–316, 1990.
[50] D. von de Linde, "Characterization of the noise in continuously operating mode-locked laser," *Appl. Phys. B*, vol. 39, pp. 201–217, 1985.
[51] H. Shang, "Chromatic dispersion measurement by white-light interferometry on meter-length single-mode optical fibers," *Electron. Lett.*, vol. 17, pp. 603–605, 1981.
[52] J. Stone and D. Marcuse, "Direct measurement of second-order dispersion in short optical fibers using white-light interferometry," *Electron. Lett.*, vol. 20, pp. 751–752, 1984.
[53] L. G. Cohen, "Comparison of single-mode fiber dispersion measurement techniques," *J. Lightwave Technol.*, vol. 3, pp. 958–966, 1985.

Brandon C. Collings was born in Bethesda, MD, in 1972. He received the B.S. degree in physics and mathematics from Hamilton College, Clinton, NY, in 1994, and the M.S. degree in electrical engineering from Princeton University, Princeton, NJ, in 1996, where he is currently pursuing the Ph.D. degree.

His research is concentrating on passively modelocked ultrafast solid-state and fiber lasers and optical nonlinearities.

Mr. Collings was the recipient of the 1995 Apker Award for his work on avalanche upconversion in rare earth doped crystals. He is a member of the OSA and IEEE-LEOS.

Keren Bergman (S'87–M'93–S'94–M'95) received the B.S. degree from Bucknell University, Lewisburg, PA, in 1988, and the S.M. and Ph.D. degrees from the Massachusetts Institute of Technology, Cambridge, MA, in 1991 and 1994, respectively, all in electrical engineering.

At Bucknell, she was an Eastman Kodak Scholar, and at MIT, a General Electric Fellow during the academic year 1988–1989, and in 1991, a recipient of the AT&T Laboratories Fellowship. She is currently an Assistant Professor of Electrical Engineering at Princeton University and a member of the Advanced Technology Center for Photonics and Optoelectronic Materials (ATC/POEM). Her research interests range from fundamental studies of quantum noise and nonlinear processes associated with short-pulse propagation in fibers, to photonic switching devices, high bit-rate laser sources, and optical networks for massively parallel performance computing.

Dr. Bergman is a Member of the OSA, Tau Beta Pi, and Sigma Chi. She was elected to the IEEE/LEOS Board of Governors for the 1996–1999 term.

S. T. Cundiff, photograph and biography not available at the time of publication.

Sergio Tsuda was born in Campinas-SP, Brazil, in 1963. He received the B.S., M.S., and Ph.D. degrees in physics from the University of Campinas (UNICAMP), Brazil, in 1986, 1991, and 1994, respectively. His Ph.D. research was in ultrafast all-optical switching and optical nonlinearities in semiconductor-doped glasses and quantum dots.

He worked as a visiting Post-Doctoral Researcher at AT&T/Lucent Technologies–Bell Laboratories, Holmdel, NJ, from 1994 to 1996, investigating and developing ultrafast diode-pumped solid-state lasers and applications. His research interests include ultrafast diode-pumped solid state lasers, nonlinear optics, ultrafast spectroscopy, optoelectronic devices and optical telecommunication devices and systems.

Dr. Tsuda is a member of the Optical Society of America and IEEE LEOS.

J. Nathan Kutz (M'96) was born in Cavalier, ND, on October 1, 1968. He received the B.S. degree in physics and mathematics from the University of Washington, Seattle, WA, in 1990 and the Ph.D. degree in applied mathematics from Northwestern University, Evanston, IL, in 1994.

From 1994 to 1995, he was a Post-Doctoral Fellow at the Institute for Mathematics and its Applications, at the University of Minnesota, Minneapolis. Since then, he has been a National Science Foundation University–Industry Post-Doctoral Fellow at the Program in Applied and Computational Mathematics, Princeton University, Princeton, NJ, and Bell Laboratories, Lucent Technologies, and AT&T Research, Murray Hill, NJ, where he has conducted research on mode-locked fiber lasers, nonlinear optical switches, dispersion managed pulse propagation, and nonlinear effects in fiber gratings.

Dr. Kutz is a member of OSA and SIAM.

J. E. Cunningham received the Ph.D. degree and Post-Doctorate work in physics at the University of Illinois at Urbana-Champaign.

After graduation, joined the Advanced Photonics Laboratory of AT&T Bell Laboratories in 1985 (now Lucent Technologies). At AT&T and Lucent, he developed advanced crystal growth methods for producing semiconducting materials in applications ranging from quantum transport at the nanoscale limits to state of the art devices in communication sciences. His current material research interests are exploiting heteroepitaxial materials for advanced photonics and modulator applications. His technological interest focus on developing materials/devices and components for the next generation of communication systems.

W. Y. Jan, photograph and biography not available at the time of publication.

M. Koch was born in Marburg, Germany, in 1963. He received the Diploma and the Ph.D. degree from the University of Marburg in 1991 and 1995, respectively.

From 1995 to 1996, he was a Post-Doctoral Fellow in the Advanced Photonics Research Department at Bell Laboratories/Lucent Technologies, Holmdel, NJ. At present, he is with the Ludwig–Maximilians-University of Munich, where he is working toward his habilitation. His research interests include ultrafast spectroscopy on semicondcutors, semiconductor heterostructures, and terahertz time-domain spectroscopy.

W. H. Knox was born in Rochester, NY. He received the B.S. and Ph.D. degrees from the Institute of Optics, University of Rochester, in 1983.

He worked as a Post-Doctoral Member of the Technical Staff at AT&T Bell Laboratories, Holmdel, NJ, from 1984 to 1985, and is currently a Distinguished Member of the Technical Staff in the Advanced Photonics Research Department, Bell Laboratories, Lucent Technologies. His research interests include the physics of quantum-confined semiconductors, nonlinear optics, femtosecond spectroscopic and optoelectronic measurements, ultrafast lasers, WDM communications systems, applications of ultrafast science and technology, coherence properties of optical materials and fields, and optics education. He is the author of more than 90 scientific papers and several book chapters.

Dr. Knox is a Fellow of the American Physical Society, a Fellow of the Optical Society of America, and a member of the OSA Fellows Committee. He has also received the 1990 National Academy of Sciences Award for Initiatives in Research. He served as Program Co-Chair of the 1994 Ultrafast Phenomena Conference, Program Chair of the 1995 Quantum Optoelectronics Conference, and General Co-Chair of the 1996 Ultrafast Phenomena Conference, Program Co-Chair of CLEO 1997, and will be the Program Co-Chair of Nonlinear Optics 1998.